

Generalized Composite Mangrove Index for Mapping Mangroves Using Sentinel-2 Time Series Data

Zhaohui Xue , Member, IEEE, and Siyu Qian 

Abstract—Monitoring mangroves is critical to protect the coastal ecosystems. Some studies resorted to remote sensing for constructing mangrove indices (MIs). However, there are still some drawbacks in existing MIs. On the one hand, difficulty still persists in distinguishing mangroves from nonmangrove vegetation and nonvegetated areas at the same time. On the other hand, the existing MIs have not fully utilized the phenological trajectories, which can greatly help to distinguish mangroves from other land covers. To overcome these issues, we built a novel mangrove index, namely generalized composite mangrove index (GCMI) by compositing vegetation indices (VIs) and water indices (WIs) based on Sentinel-2 time series data. Firstly, to determine the optimal indices, a similarity trend distance (ST distance) measure was proposed based on Pearson correlation coefficient and dynamic time warping (DTW). Secondly, in order to optimize the weights of selected indices, a population reconstruction genetic algorithm (PRGA) was designed. Finally, mangroves were mapped by feeding the time series of GCMI into random forest classifier. Experiments conducted over three areas along the southern coast of China demonstrate that: 1) GCMI enhances the separability between mangroves and other land covers compared to the existing VIs, WIs, and MIs, with an averaged overall accuracy of 91.45%; 2) ST distance outperforms Euclidean distance, Cosine distance, Pearson correlation coefficient, and DTW in optimizing the weights of GCMI; 3) PRGA greatly improves the probability of attaining global optimal result. The innovation lies in the presented GCMI considering both the vegetation trajectory information and water inundation using time series.

Index Terms—Generalized composite mangrove index (GCMI), mangrove mapping, random forest (RF), remote sensing.

I. INTRODUCTION

MANGROVES, growing in tropical and subtropical regions, are adapted to live in land-sea interface areas. Mangroves are playing an important role in maintaining the productivity and biodiversity of coastal wetlands, protecting coastal seawalls, preventing wind and waves, etc. However, mangrove ecosystem is easily damaged by human activities and

Manuscript received 26 January 2022; revised 15 April 2022 and 3 May 2022; accepted 17 June 2022. Date of publication 21 June 2022; date of current version 4 July 2022. This work was supported in part by the National Natural Science Foundation of China under Grant 41971279 and in part by the Fundamental Research Funds for the Central Universities under Grant B200202012. (*Corresponding author: Zhaohui Xue.*)

The authors are with the School of Earth Sciences and Engineering, Hohai University, Nanjing 211100, China, and also with the Jiangsu Province Engineering Research Center of Water Resources and Environment Assessment Using Remote Sensing, Hohai University, Nanjing 211100, China (e-mail: zhaohui.xue@hhu.edu.cn; qsy108@163.com).

Digital Object Identifier 10.1109/JSTARS.2022.3185078

hard to rehabilitation due to its poor self-recovery ability [1]–[5]. Therefore, proper utilization and protection of mangrove ecosystem has become the focus of the worldwide attention.

Reliable and accurate mangrove mapping is the basis and prerequisite for protection and restoration. However, mangroves are usually distributed in harsh coastal conditions, making it difficult to survey in large-scale. Remote sensing has the advantages of surveying in large and inaccessible areas, analyzing in time, and acquiring the information without disturbing the environment, which has become an important tool of mangrove mapping [6]–[9]. Among various remote sensing data, Sentinel-2 multispectral instrument (MSI) has been widely used in mangrove mapping due to its high spatial and temporal resolution [10]–[13]. However, mapping mangroves by using remote sensing has two difficulties: 1) mangroves are highly similar to terrestrial vegetation, and there is no natural isolation in geographical space between them, leading to misclassification and omission; 2) mangroves are submerged by periodic tides, resulting in extracting mangroves periodically flooded a tough task. In order to solve the above two-sided difficulties, existing studies mainly focused on: 1) exploring appropriate classification models; 2) extracting more discriminating features; and 3) constructing novel MIs.

Exploring classification models is an effective way since it can make up the limitations of previous proposed classifiers. Various related studies mainly used ensemble learning [14]–[16], support vector machine (SVM) [17]–[19], decision tree (DT) [20], [21], and deep learning [22]–[24].

- 1) Ensemble learning uses multiple learning algorithms to obtain better results. For example, Li and Hughes [14] applied bagging, boosting, and stacking to map wetland distribution in Manning River Estuary. Moreover, random forest (RF) is now commonly applied in remote sensing, such as Navarro *et al.* [15] used RF to map mangroves in South-Eastern Australia from 1991 to 2015. Further on, considering an ensemble of machine learning methods is more accurate than a single model, Liu *et al.* [16] ensembled RF, gradient boosting machine, and neural network (NN) to map mangrove at high accuracies.
- 2) SVM is also widely used because it can get great classification results from complex and noisy data. Nwobi *et al.* [17] mapped mangroves using maximum likelihood (ML) and SVM methods, which found that SVM performed better than ML. Likewise, Quang *et al.* [18] investigated the performance of NN, DT, RF, and SVM to classify mangroves,

which also concluded that SVM was the most accurate classifier.

- 3) DT is easy to be implemented, and it has high interpretability. Zhang *et al.* [20] developed DT based on multitudinal Landsat 5 thematic mapper (TM) data and a digital elevation model to map mangrove forests. Furthermore, by using DT, McCarthy *et al.* [21] not only mapped the extent of mangroves, but also distinguished between healthy and degraded mangroves.
- 4) Deep learning is gaining widespread popularity in the remote sensing community recently since it can extract high-level features directly from the raw input data. For example, Iovan *et al.* [22] designed a model based on deep convolutional neural network (CNN) using WorldView-2 and Sentinel-2 images. Guo *et al.* [23] also utilized CNN, but the difference is that they embedded three modules to improve performance.

To conclude, utilizing a proper classification method is highly important to distinguish mangroves. Besides considering classification methods, extracting more discriminating features can help to enhance the difference between mangroves and other land covers, because diverse features can provide complementary information.

- 1) On the one side, extracting features from single-source optical data is effective to get distinguishing features. Since time series can demonstrate phenological information of different land covers, Lymburner *et al.* [25] used Landsat dense time series as features to quantify the mangrove extent in Australia. With the development of remote sensing satellite technology, the increased spatial resolution is expected to obtain a more detailed mangrove mapping. Therefore, Wang *et al.* [26] selected features from Landsat 8, Sentinel-2, and Pliades-1 based on RF to map mangroves in a higher spatial resolution. Due to more spectral details are provided from hyperspectral data, Li *et al.* [27] mapped multilayered mangrove by using airborne hyperspectral images.
- 2) On the other side, as optical data are easily influenced by weather and illumination conditions, using multisource data can resolve the problem to some extent. For example, Bunting *et al.* [28] used features from Advanced Land Observing Satellite (ALOS) Phased Array-type L-band Synthetic Aperture Radar (SAR) (PALSAR) to distinguish mangroves from coastal areas firstly, then used features from Landsat to differentiate between mangroves and adjoining terrestrial forests.
- 3) In addition, some studies used multitemporal features from multisource data with a view to the special phenology of mangroves [29]. For example, Hu *et al.* [30] used Sentinel-1 SAR and Sentinel-2 MSI time series imagery as input features of RF to classify mangroves in China. Instead of directly regarding time series as features, Chen *et al.* [31] proposed a new classification algorithm which mapped mangroves by identifying the greenness, canopy coverage, and tidal inundation from time series of Landsat data and Sentinel-1 A. What is more, Zhao and Qin [32] used the temporal profiles derived from a multisource

and multitemporal satellite to enhance the discrimination between mangroves and other land covers. Ghorbanian *et al.* [33] also generated seasonal features from Sentinel-1 and Sentinel-2 satellite images to obtain a more reliable mangrove ecosystem map.

To sum up, the abundant features can be extracted from multi-source and multitemporal data, assisting in masking mangroves from other vegetation and tide more easily. What is more, many indices are designed to get specific information, e.g., normalized difference vegetation index (NDVI) [34] can estimate the density of green, and leaf area index [35] can highlight the leaf greenness. Therefore, constructing MIs is also feasible to take full advantage of mangrove characteristics.

- 1) In the aspect of distinguishing mangroves from terrestrial vegetation, Gupta *et al.* [36] utilized the correlation between NDVI and normalized difference water index (NDWI) to develop a new index, namely combined mangrove recognition index (CMRI). Rather than constructing index based on the existing indices, Baloloy *et al.* [37] used Sentinel-2 data to design the mangrove vegetation index (MVI) specifically for mangrove mapping.
- 2) In the aspect of differentiating between mangroves and tides, many scholars used mult tide data to relieve this issue. For example, Jia *et al.* [38] established the inundated mangrove forest index (IMFI) based on high tide and low tide lines, which successfully extracted the mangroves submerged by seawater. Furthermore, Xia *et al.* [39] utilized the near-infrared band, which is more likely to reflect spectral differences in high tide and low tide periods, to construct submerged mangrove recognition index (SMRI). Particularly, Li *et al.* [40] proved the robustness of SMRI as an effective indicator to detect submerged mangroves in both high and medium spatial resolution satellite images. Likewise, Xu *et al.* [41] proposed normalized intertidal mangrove index (NIMI) by comparing and analyzing the spectral characteristics of exposed mangroves, submerged mangroves, and seawater bodies.
- 3) In the aspect of extracting mangroves from nonmangrove vegetation and tides simultaneously, Kumar *et al.* [42] designed mangrove probability vegetation index (MPVI), normalized difference wetland vegetation index, and shortwave infrared absorption depth based on EO-1 Hyperion data.

Consequently, it is useful to construct an effective index in order to precisely map mangroves. However, there are still some deficiencies in the existing MIs. For one side, although MIs can distinguish mangroves from nonmangrove vegetation and tidal, it is still difficult to distinguish mangroves from other vegetation and nonvegetated simultaneously. For another side, the existing MIs have not fully utilized the phenological trajectories from the multitemporal data.

In this article, we constructed a novel and effective generalized composite mangrove index (GCMI) composed by VIs and WIs with Sentinel-2 time series. Firstly, in order to determine the optimal indices, we proposed an similarity trend distance (ST) measure based on Pearson correlation coefficient and dynamic

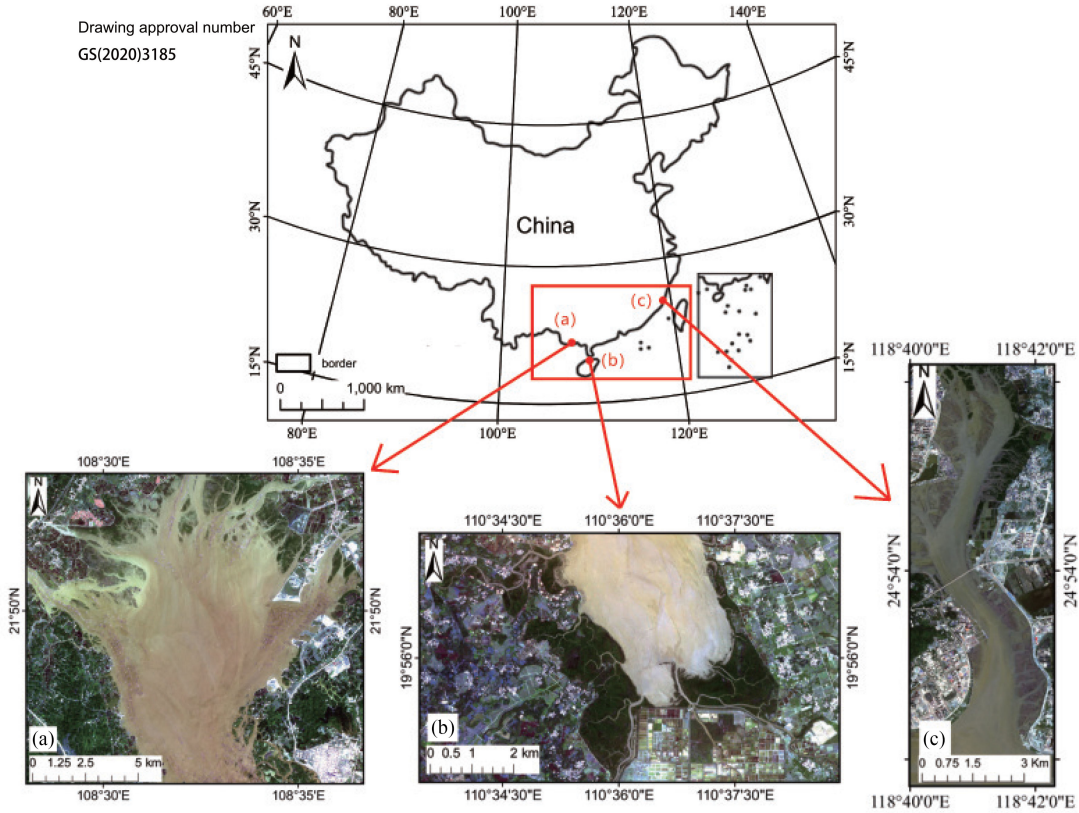


Fig. 1. Study area situated in south coastal region of China. (a) Maowei Sea in Guangxi Province. (b) Dongzhai Port in Hainan Province. (c) Quanzhou Bay in Fujian Province. Note that the base China map with approval number GS(2020)3185 has not been made any modification.

time warping (DTW), which was used to select indices to construct the GCMI. Secondly, since the weights of the selected indices were undetermined, population reconstruction genetic algorithm (PRGA) was designed to get the optimal weights. Finally, the time series of GCMI were used as the inputs of RF to get mangrove maps of Maowei Sea, Dongzhai Port, and Quanzhou Bay at 10-m spatial resolution in 2020.

This rest of this article is organized as follows. Section II presents the study area and data. The methodologies are illustrated in Section III. The experimental results are presented and analyzed in Section IV. The discussion is drawn in Section V. Finally, Section VI concludes this article.

II. STUDY AREA AND DATA

A. Study Area

The study area is located in the south coastal regions of mainland China, including Maowei Sea in Guangxi Province [see Fig. 1(a)], Dongzhai Port in Hainan Province [see Fig. 1(b)], and Quanzhou Bay in Fujian Province [see Fig. 1(c)]. The climates in these areas vary from tropical monsoon to subtropical monsoon climate with high temperature and rainfall in summer, whereas low temperature and little rainfall in winter. Port development, rapid economic growth as well as abundant habitats of microbial communities have made mangrove ecosystems the priorities of the coastal management programs [38], [43].

Owing to its north-limit distribution, the mangrove forests in China are dominated by low-temperature tolerant species such as

Kandelia obovata, *Aegiceras corniculatum*, and *Avicennia marina*. The majority of mangrove forests in China are distributed in estuaries, and characterized by abundant inputs of freshwater and nutrients [44].

Maowei Sea is the largest and most typical mangrove forest area in China, which is the ideal place for mangrove introduction, cultivation experiment and development. The representative mangrove growth types in this area is *Bruguiera gymnorhiza*, *Kandelia candel*, *Rhizophora stylosa*, *Acanthus ilicifolius*, etc., accounting for 43.2% of mangrove species in China. Dongzhai Port is the largest coastal mudflat forest in China with abundant species genes and resources. The reserve is rich in mangrove species and accounts for 97% of mangrove species in China, including *Nypa fruticans*, *Sonneratiaovata*, *Xylocarpus granatum*, etc. Quanzhou Bay has a piece of native mangrove where it is rich in wetland resources. The representative mangrove growth types in this area are *Kandelia candel*, *Aegiceras Gaertn*, *Avicennia marina*, etc. The above three nature mangrove reserves have different representative mangrove growth types and various ecological environments. Therefore, we conducted our research based on the above three study areas.

B. Remote Sensing Data

In this article, Sentinel-2 MSI data during 2019 to 2020 was obtained, and the numbers of images in each region are listed in Table I. The data preprocessing was implemented on Google Earth Engine (GEE) platform, where Sentinel-2 data

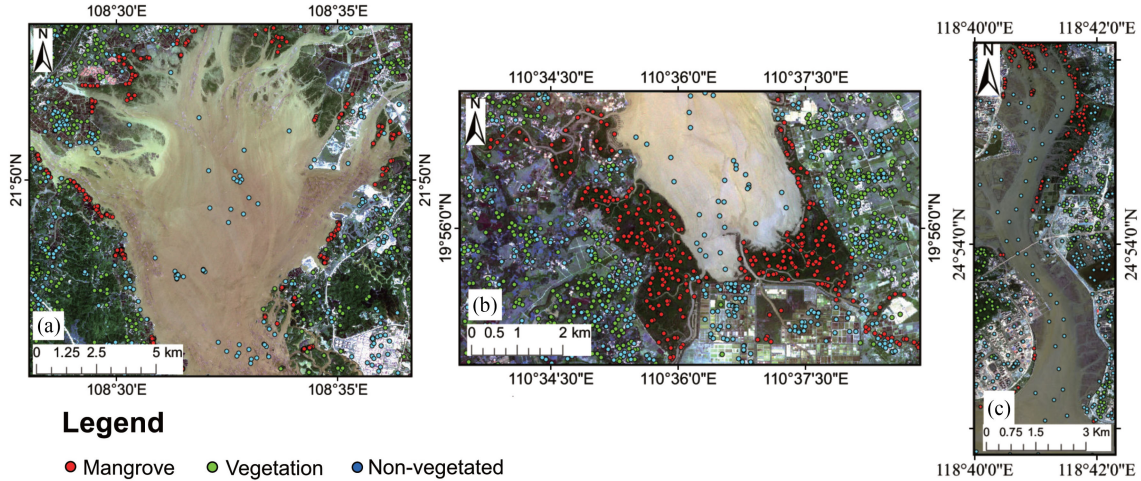


Fig. 2. Distribution map of samples in different study areas.

TABLE I
SENTINEL-2 MSI DATA

Study area	Site name	Number of images		
		2019	2020	Total
(a)	Maowei Sea	124	150	274
(b)	Dongzhai Port	73	75	148
(c)	Quanzhou Bay	72	73	145

TABLE II
NUMBER OF SAMPLES IN EACH STUDY AREA

Study area	Site name	Number of samples		
		Mangrove	Vegetation	Non-vegetated
(a)	Maowei Sea	300	427	400
(b)	Dongzhai Port	333	492	466
(c)	Quanzhou Bay	201	317	300

have been radiometric corrected and there is no geometric distortion. Therefore, radiometric calibration, atmospheric correction, and geometric correction were not required. In order to get high-quality time series, we made the following preprocess. Firstly, a band logic operation was used to remove cloud according to the quality evaluation information of the dataset. Secondly, a linear interpolation was used to fill gaps in time series after removing cloud. Thirdly, to unify the time interval of data and weaken the influence of cloudy, the maximum synthesis method was used to construct a seven-day time series. Finally, an S-G filter was used to smooth the time series, aiming to eliminate outliers in time series.

C. Reference Data

Reference data was randomly sampled as evenly as possible throughout the research sites covering mangroves (hereafter named “Mangrove”), nonmangrove vegetation (hereinafter named “Vegetation”), and the regions without vegetation (hereafter named “Nonvegetated”). Among them, the mangrove samples were selected referring to the Global Mangrove Classification products (with 10-m resolution and overall accuracy of 91.62%) released by [45] and Zhao’s sample set [46]. The above

two datasets were acquired on Science Data Bank¹. And the other two types were selected by visual interpretation based on Google Earth images. Further on, in order to avoid mixed samples, we tried to select samples from the center of the area. The number of samples for each study area is reported in Table II, and the distribution maps of samples are shown in Fig. 2.

III. METHODOLOGY

A flowchart of the presented methodology is illustrated in Fig. 3. Firstly, Sentinel-2 dataset after preprocessing was used to construct time series for each index. Secondly, the optimal indices were selected according to ST distance. Thirdly, by using PRGA, the weights of the GCMI were optimized. Finally, RF was adopted to classify mangroves with the time series of GCMI as the inputs.

A. Generalized Composite Mangrove Index

1) *Indices Calculation:* Since the mangroves and other land covers, especially nonmangrove vegetation, have same trend in most wavelengths (see Fig. 4), we constructed GCMI based on the existing indices rather than based on bands. Considering that mangroves are evergreen broad-leaved forests and their growth environment is influenced by tides, mangroves have special vegetation information and tidal inundation information. In order to make full use of the above information, we considered both vegetation indices (VIs) and water indices (WIs) to map mangroves (Table III). Among them, VIs not only can distinguish mangroves from nonvegetated area, but also from other deciduous vegetation to a certain extent. What is more, mangroves are submerged by tides periodically, thus the WIs are added to distinguish mangroves from nonmangrove vegetation.

2) *GCMI Construction:* Since the information of mangroves described by single index is limited, we considered compositing different indices to increase the separability between mangroves and other land covers. Considering too much of the indices may

¹[Online]. Available: <https://www.scidb.cn/>

TABLE III
INDICES INVOLVED IN THIS STUDY

Type	Name	Definition
VIs	Normalized difference vegetation index (NDVI) [34]	$\frac{\rho_{Nir} - \rho_{Red}}{\rho_{Nir} + \rho_{Red}}$
	Enhanced vegetation index (EVI) [47]	$\frac{2.5(\rho_{Nir} - \rho_{Red})}{\rho_{Nir} + 6\rho_{Red} - 7.5\rho_{Blue} + 1}$
	Difference vegetation index (DVI) [48]	$\rho_{Nir} - \rho_{Red}$
	Green normalized difference vegetation index (gNDVI) [49]	$\frac{\rho_{Nir} - \rho_{Green}}{\rho_{Nir} + \rho_{Green}}$
WIs	Land surface water index (LSWI) [50]	$\frac{\rho_{Nir} - \rho_{Swir}}{\rho_{Nir} + \rho_{Swir}}$
	Normalized difference water index (NDWI) [51]	$\frac{\rho_{Green} - \rho_{Nir}}{\rho_{Green} + \rho_{Nir}}$
	Enhanced water index (EWI) [52]	$\frac{\rho_{Green} - \rho_{Nir} - \rho_{Swir}}{\rho_{Green} + \rho_{Nir} + \rho_{Swir}}$
	Revised normalized different water index (RNDWI) [53]	$\frac{\rho_{Swir} - \rho_{Red}}{\rho_{Swir} + \rho_{Red}}$
MIs	Combined mangrove recognition index (CMRI) [36]	$NDVI-NDWI$
	Mangrove vegetation index (MVI) [37]	$\frac{\rho_{Green} - \rho_{Nir}}{\rho_{Green} + \rho_{Nir}}$
	Iundated mangrove forest index (IMFI) [38]	$\frac{\rho_{Blue} + \rho_{Green} - 2\rho_{Nir}}{\rho_{Blue} + \rho_{Green} + 2\rho_{Nir}}$
	Normalized intertidal mangrove index (NIMI) [41]	$\frac{3\rho_{Red} - (\rho_{RedEdge2} + \rho_{RedEdge3} + \rho_{Nir})}{3\rho_{Red} + \rho_{RedEdge2} + \rho_{RedEdge3} + \rho_{Nir}}$

Note: Nir: Near infrared band, Red: red band, Green: green band, Blue: Blue band, Swir: Short infrared band, Red Edge 2: Red Edge 2 band, Red Edge 3: Red Edge 3 band.

lead to information redundancy, we only selected two VIs and WIs to construct GCMI, which is given in

$$GCMI = \frac{A \times VI_A + B \times VI_B}{C \times WI_A + D \times WI_B} \quad (1)$$

where VI_A and VI_B are the two optimal VI, and WI_A and WI_B are the two optimal WI.

The numerator of the equation ($VI_A + VI_B$) enhanced the differences of vegetation greenness between mangrove forests and nonvegetated area. Whereas the denominator of the equation ($WI_A + WI_B$) expressed the special moisture information of mangroves, which is quite different from other vegetation. GCMI measured the probability of mangrove pixels by utilizing both the VIs and WIs to highlight mangroves' greenness and moisture, respectively. Therefore, GCMI can separate mangroves from other land covers simultaneously. Besides, there are also some salt marsh plants (like spartina alterniflora) distributed in the tidal flats, which might be similar to mangroves in WIs. However, this type of vegetation has an obvious seasonal characteristic that can be distinguished by VIs easily.

B. Similarity Trend Distance

To construct GCMI, it is necessary to select the optimal indices with large discrimination. Therefore, a suitable measure is required to describe the difference between time series. Some commonly used distances measures are Cosine distance, Euclidean distance, Pearson correlation coefficient, and dynamic time warping (DTW) [54], etc. Since the input time series was the average values of a land cover, the distance measure should focus more on the trend rather than the value. Therefore, the above metrics are not quite suitable. For example, Euclidean distance only focuses on the difference between two values whereas Cosine distance only considers the angle difference. Pearson correlation coefficient does not fully consider the trend of time series and DTW distance needs to unify scales of the input before comparing. Furthermore, the above metrics use a single criterion to determine the difference, which may lead to one-sided effects. Therefore, in this study we intend to define a

novel distance measure, namely ST distance, which can consider both similarity and trend of time series.

ST distance was composed of two parts: 1) one part aiming to measure similarity of time series; 2) the other part aiming to determine trend differences of time series. In the first part, we chose the Pearson correlation to describe the similarity between time series since it has been standardized, which pays less attention to the value differences. In the second part, we constructed the trend subsequence of time series firstly, then used DTW to calculate distance between the subsequences since the dimension of subsequences are variant.

Given a time series X_n [(2)], the trend subsequence of time series can be constructed as follows (see Fig. 5):

$$X_n = \{x_{n_1}, x_{n_2}, x_{n_3}, \dots, x_{n_{i-1}}, x_{n_i}\} \quad (2)$$

where i is the length of the input time series and x_{n_i} is the value in X_n .

- Using a sliding window to calculate the difference between two adjacent x_{n_i} , which is given in

$$\begin{aligned} X_d &= \{x_{n_2} - x_{n_1}, x_{n_3} - x_{n_2}, \dots, x_{n_i} - x_{n_{i-1}}\} \\ &= \{x_{d_1}, x_{d_2}, x_{d_3}, \dots, x_{d_{j-1}}, x_{d_j}\} \end{aligned} \quad (3)$$

where x_{d_j} is the difference of two adjacent x_{n_i} , obviously $j = i - 1$.

- Judging the state of each x_{d_i} , where x_{d_j} greater than 0 (the rising state) is 1, x_{d_j} less than 0 (the falling state) is -1, and x_{d_j} equal to 0 (the invariable state) is 0 as

$$X_s = \frac{X_d}{|X_d|} = \{x_{s_1}, x_{s_2}, x_{s_3}, \dots, x_{s_{j-1}}, x_{s_j}\} \quad (4)$$

where x_{s_j} represents the state of x_{d_j} .

- Merging the adjacent x_{s_j} that are in the same state as

$$\begin{aligned} X_t &= \left\{ \sum_{i=1}^{m_1} x_{s_j}, \sum_{i=m_1+1}^{m_2} x_{s_j}, \dots, \sum_{i=m_q+1}^{m_p} x_{s_j} \right\} \\ &= \{x_{t_1}, x_{t_2}, x_{t_3}, \dots, x_{t_{k-1}}, x_{t_k}\} \end{aligned} \quad (5)$$

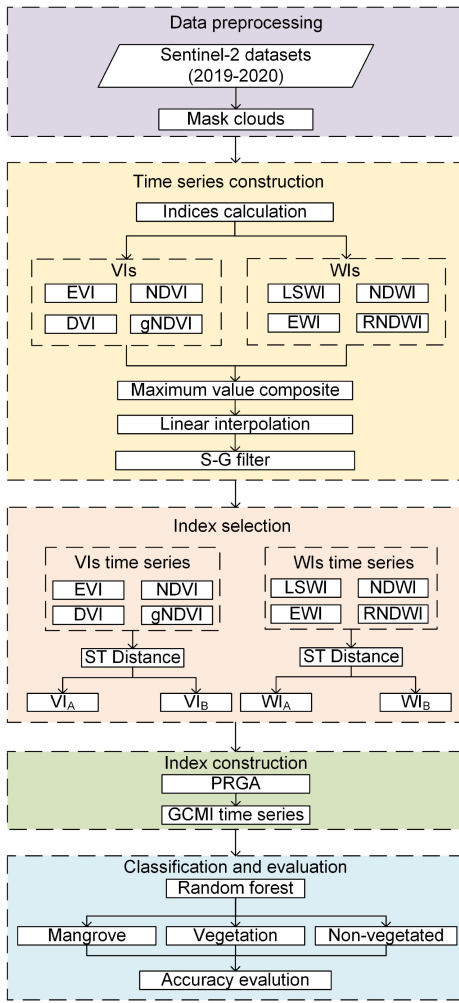


Fig. 3. Flowchart of the presented methodology.

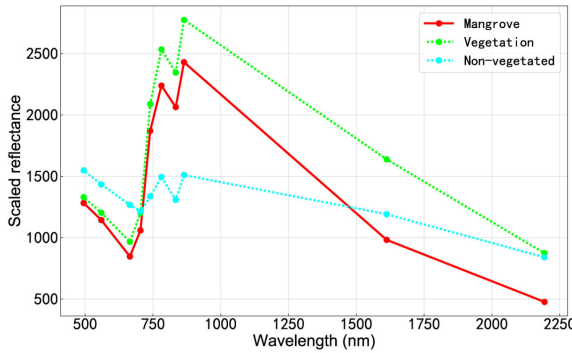


Fig. 4. Spectral differences between mangroves and other land covers.

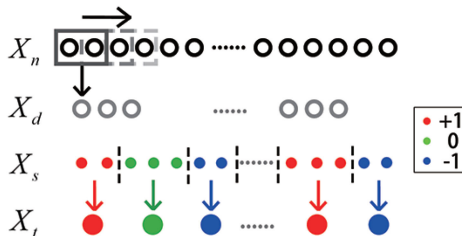


Fig. 5. Subsequence construction.

TABLE IV
CODING METHOD

Gene	01	02	03	...	25	26	...	48	49	50
Value	0.1	0.2	0.3	...	25	26	...	48	49	50

TABLE V
ST DISTANCE OF DIFFERENT INDICES IN MAOWEI SEA

Index	Mangrove vs. Vegetation	Index	Mangrove vs. Non-vegetated
EVI	0.919	DVI	2.926
LSWI	8.781	EVI	4.635
NDWI	0.603	NDVI	2.714
RNDWI	1.33	gNDVI	5.102

The indices with bold typeface are selected to construct GCMI in Maowei Sea.

where m_p is the length of adjacent x_{s_j} in the same state and X_t is the trend subsequence of X_n .

In this context, ST distance can be formulated as

$$ST = (1 - |C_{X_n X_{n'}}|) \times D_{X_t X_{t'}} \quad (6)$$

where X_n and $X_{n'}$ are the pair of time series to be compared correspondingly, X_t and $X_{t'}$ are the trend subsequence of the X_n and $X_{n'}$, respectively. Besides, in order to make the dissimilar pair of time series has the higher value of ST distance, we used one minus the absolute value of Pearson correlation as the first part of ST distance. Consequently, when ST is larger, then the difference between the two time series would be greater. According to ST distance, the VIs and WIs with greater differentiation will be selected to construct GCMI.

C. Population Reconstruction GA

Intuitively, genetic algorithm (GA) [55] can be used to optimize the undetermined weights of the GCMI. GA is a heuristic search algorithm based on Darwin's theory of evolution, which searches for the optimal value by imitating the genetics and evolution in biology [56]. But the classical GA still has some limitations. For example, it probably cannot get the optimal solution because of the premature convergence. In addition, the optimization results greatly depend on the initial value and the effectiveness of fitness function [57]. To overcome the above problems, we improved the classical GA by reconstructing population, i.e, PRGA. PRGA can get optimal value more probably in the same condition. The flow chart of PRGA is shown in Fig. 6.

Firstly, the given information would be encoded in a particular bit string. Encoding schemes play an important role in most of computational problems since it can directly affect overall calculation speed of the algorithm and whether optimal result can be found. Considering the simplicity of GCMI, the search range of the undetermined weights was specified as (0,5] with an interval of 0.1. Therefore, we adopted an efficient and simple coding method which is based on permutation (Table IV). After encoding, genes were selected randomly according to initial population size. So far, the population had been initialized.

Secondly, genes need to be evaluated by a fitness function. We chose ST distance as the fitness function, which can better evaluate the differences between time series due to jointly considering both similarity and trend. The fitness function used in

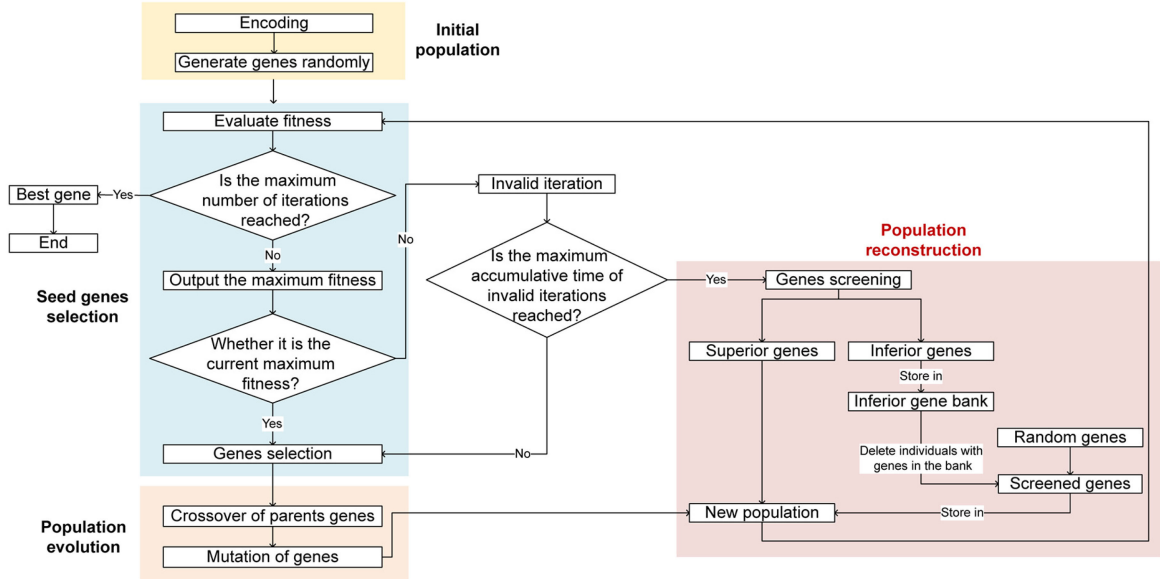


Fig. 6. PRGA.

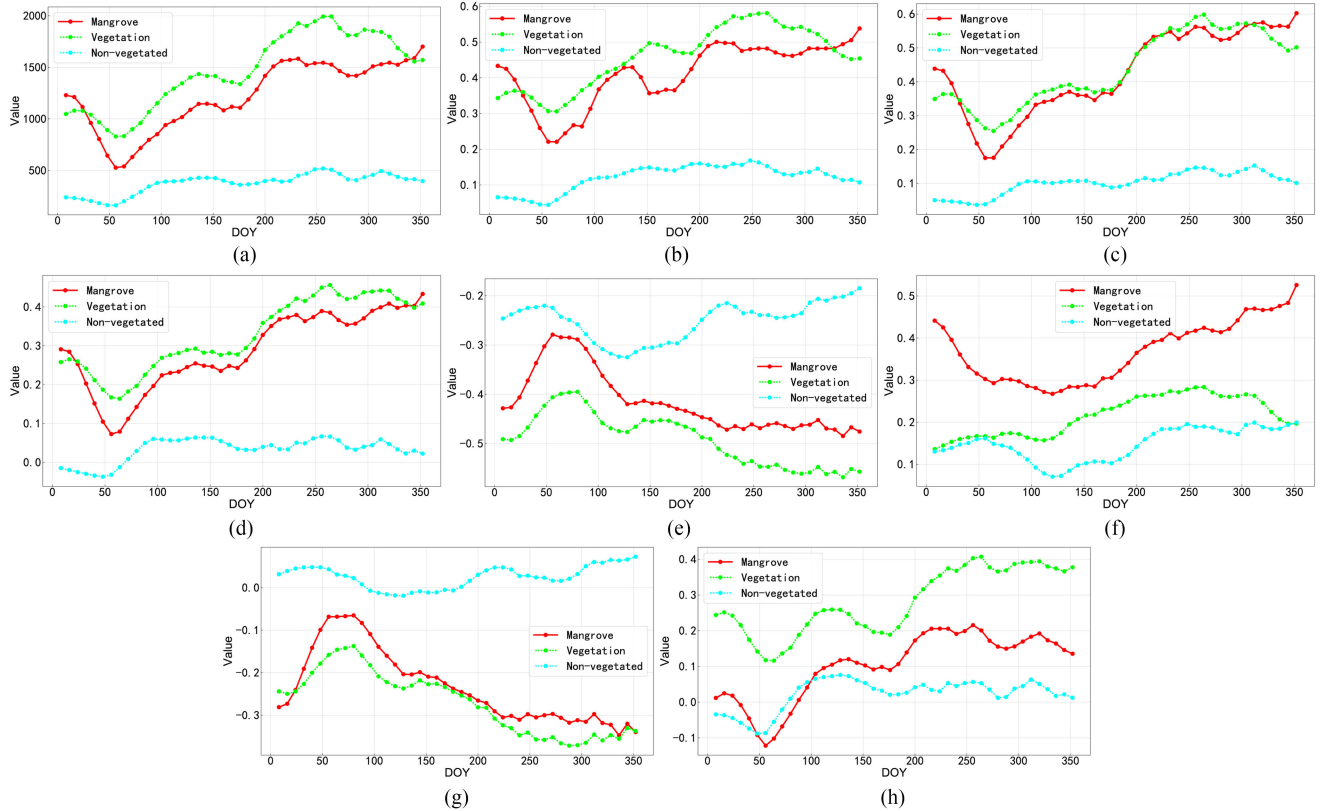


Fig. 7. Various time series of different land covers (Note: DOY means day of year). (a) DVI. (b) EVI. (c) NDVI. (d) gNDVI. (e) EWI. (f) LSWI. (g) RNDWI. (h) NDWI.

PRGA is formulated as

$$f = \frac{2}{\frac{1}{ST_{mv}} + \frac{1}{ST_{mn}}}, \quad (7)$$

where ST_{mv} is the ST distance between time series of mangrove and vegetation, and ST_{mn} is the ST distance between time series of mangrove and nonvegetated.

Thirdly, the population needed to be evolved according to f . We chose roulette wheel as selection techniques, simulated

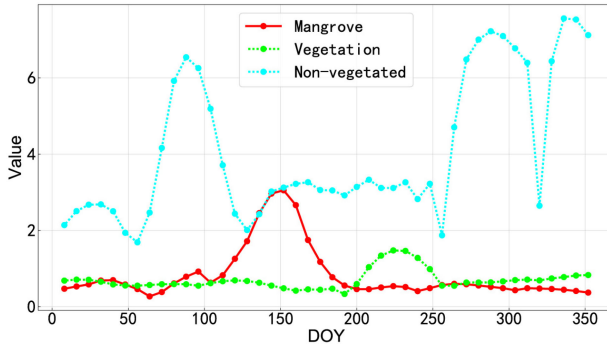


Fig. 8. GCMI time series of different land covers.

TABLE VI
PARAMETERS OF PRGA IN MAOWEI SEA

Parameter	Value
Maximum number of iteration	50
Population size	1000
Maximum number of invalid iteration	3
Crossover rate	0.8
Mutation rate	0.03

TABLE VII
GA OPTIMIZATION RESULTS IN MAOWEI SEA

Method	Run	A	B	C	D	Fitness	Time (s)	#†
PRGA	1	3.4	2.9	4.3	1.1	15.363	211.52	34
	2	3.4	2.9	4.3	1.1	15.363	210.63	48
	3	3.4	2.9	4.3	1.1	15.363	215.05	35
	4	2.8	2.4	4.3	1.1	15.362	209.95	/
	5	3.4	2.9	4.3	1.1	15.363	212.34	33
	6	2.8	2.4	4.3	1.1	15.362	204.61	/
	7	3.4	2.9	4.3	1.1	15.363	203.6	31
	8	4.1	3.5	4.3	1.1	15.363	205.94	/
	9	3.4	2.9	4.3	1.1	15.363	207.63	28
	10	3.4	2.9	4.3	1.1	15.363	215.11	30
GA	1	3	4.1	4.4	0.6	15.127	198.96	-
	2	4.2	3.6	4.3	1.1	15.362	200.02	-
	3	3.4	2.9	4.3	1.1	15.363	199.15	-
	4	3.4	2.9	4.3	1.1	15.363	199.3	-
	5	3.4	4.1	4.4	0.6	15.127	195.59	-
	6	3.4	4.1	4.4	0.6	15.127	199.3	-
	7	4.1	3.5	4.3	1.1	15.363	199.82	-
	8	3	4.1	4.4	0.6	15.127	197.21	-
	9	3.4	2.9	4.3	1.1	15.363	199.63	-
	10	1.1	1.5	4.4	0.6	15.127	199.4	-

† The iteration reaching to the optimal result.

The results with bold typeface indicate the optimal values.

binary crossover [58] as crossover operator, and random permutation as mutation operator.

Finally, in order to overcome the problem of premature convergence, we proposed PRGA by adding a module named population reconstruction. If it reaches the maximum accumulative time of invalid iteration, PRGA will reconstruct the population. The concrete operations of population reconstruction are as follows: 1) PRGA evaluates genes by dividing genes into the inferior and the superior. In this article, the average fitness of current population is regarded as evaluation criteria, which means that the genes greater than average are the superior and the genes lower than average are the inferior. 2) PRGA keeps superior genes and deletes inferior genes. Besides, inferior genes are stored in the inferior gene bank. 3) PRGA adds new random genes into population. Especially, new random genes are not

in the inferior gene bank to prevent repeated searches. After population reconstruction, new population is used to perform the above steps again.

Compared with classical GA, PRGA added the module of population reconstruction. Since one of the reasons of causing local optimization is the unicity in population, this module deletes the inferior genes and adds new random genes to maintain the diversity in population, which can avoid suffering from local optima problem to some extent.

D. Classification and Accuracy Assessment

After selecting indices according to ST distance and determining weights by using PRGA, the time series of GCMI were adopted for classification using RF. RF not only has high classification accuracy and less training time, but also has low sensitivity to training sample quantity, quality, and sample imbalance, which have been widely used for remote sensing image classification [59]. The study area contains three land cover types, where 60% labeled samples are randomly selected for training and the rest of 40% samples are used for test. Consumer accuracy (CA), overall accuracy (OA), and Kappa coefficient were calculated by confusion matrix as the evaluation indices.

IV. RESULTS

A. Experimental Settings

- 1) Aiming to verify the effectiveness of PRGA, we compared classical GA and PRGA.
- 2) In order to verify the effectiveness of GCMI, we compared difference vegetation index (DVI), enhanced vegetation index (EVI), Green Normalized Difference Vegetation Index (gNDVI), NDVI, enhanced water index (EWI), land surface water index (LSWI), NDWI, revised normalized different water index (RNDWI), CMRI, MVI, IMFI, and NIMI.
- 3) We evaluated the effectiveness of ST distance by comparing with Euclidean distance, Cosine distance, Pearson correlation coefficient, and DTW.
- 4) All experiments in this article were implemented on Python 3.7 under Windows 10, Intel Core i7 central processing unit (CPU), 64 GB random access memory (RAM) environment. Besides, data preprocessing and classification were achieved on GEE platform.

B. Determination of GCMI

1) *Time Series Separability Analysis:* For the purpose of selecting optimal indices to construct GCMI, we analyzed the separability of time series. Fig. 7 shows the time series of different land covers. On one hand, the time series of VIs between mangrove and vegetation are highly similar, which is difficult to distinguish mangrove from other vegetation by only using time series of VIs. Therefore, time series of VIs were mainly used to distinguish between mangrove and nonvegetated. On the other hand, the time series of WIs are quite different from other vegetation since mangroves are inundated by periodic tides. Therefore, time series of WIs are used to distinguish between mangrove and vegetation.

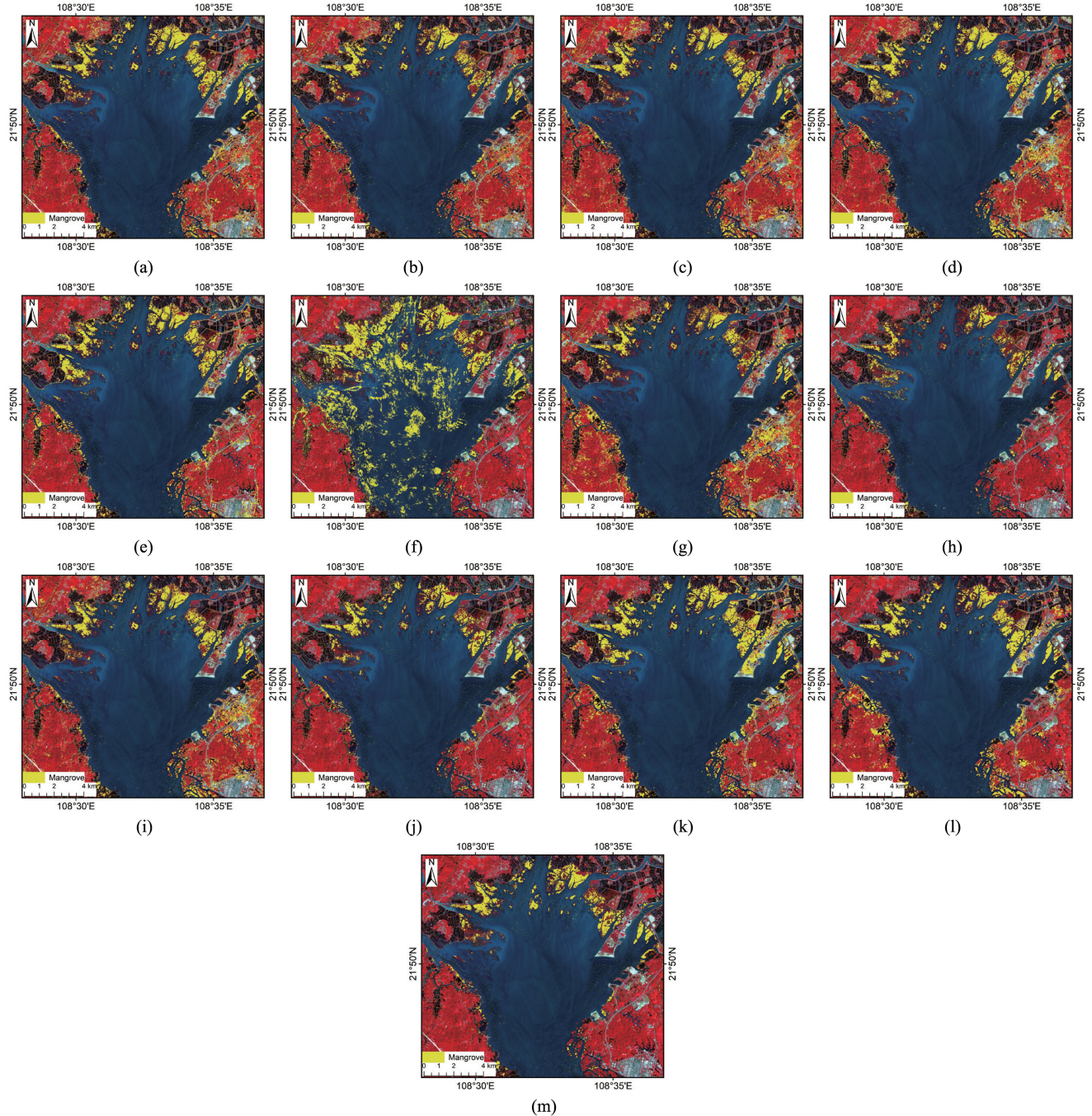


Fig. 9. Classification results based on different indices in Maowei Sea. (a) DVI. (b) EVI. (c) NDVI. (d) gNDVI. (e) EWI. (f) LSWI. (g) NDWI. (h) RNDWI. (i) CMRI. (j) MVI. (k) IMFI. (l) NIMI. (m) GCMI.

TABLE VIII
COMPARISON OF DIFFERENT FITNESS FUNCTIONS IN MAOWEI SEA

Fitness function	(A, B, C, D)	CA/%			Kappa	OA/%
		Mangrove	Vegetation	Non-vegetated		
Euclidean distance	(5.0, 5.0, 2.3, 0.8)	90.41±1.85	87.59±2.48	93.54±1.72	0.8575±0.01	90.50±0.81
Euclidean distance	(5.0, 5.0, 4.6, 1.6)	90.40±2.30	88.49±2.34	94.30±2.48	0.8654±0.02	91.03±1.37
Cosine distance	(0.1, 5.0, 2.3, 0.8)	89.58±2.70	87.78±3.23	93.11±2.17	0.8517±0.02	90.11±1.38
Pearson correlation	(0.8, 3.8, 4.5, 1.7)	89.60±3.05	89.34±3.28	94.99±2.34	0.8683±0.03	91.22±2.11
DTW distance	(5.0, 5.0, 2.3, 0.8)	90.41±1.85	87.59±2.48	93.54±1.72	0.8575±0.01	90.50±0.81
ST distance	(3.4, 2.9, 4.3, 1.1)	96.12±1.14	89.78±1.94	89.95±4.06	0.8758±0.03	91.72±1.67

The results with bold typeface indicate the highest accuracies.

TABLE IX
COMPARISON OF DIFFERENT WEIGHTS IN MAOWEI SEA

	(A, B, C, D)	CA/%			Kappa	OA/%
		Mangrove	Vegetation	Non-vegetated		
Suboptimal A	(4.1, 3.5, 4.3, 1.1)	90.19±3.40	89.80±3.03	93.55±1.87	0.8667±0.02	91.11±1.37
Suboptimal B	(2.8, 2.4, 4.3, 1.1)	88.70±2.44	88.62±4.54	93.08±1.54	0.8504±0.02	90.03±1.62
Suboptimal C	(4.2, 3.6, 4.3, 1.1)	89.02±2.12	90.06±2.58	94.58±1.63	0.8679±0.02	91.19±1.51
Optimal	(3.4, 2.9, 4.3, 1.1)	96.12±1.14	89.78±1.94	89.95±4.06	0.8758±0.03	91.72±1.67

The results with bold typeface indicate the highest accuracies.

TABLE X
COMPARISON OF CLASSIFICATION ACCURACY OF DIFFERENT INDICES IN MAOWEI SEA

	Index	CA/%			Kappa	OA/%
		Mangrove	Vegetation	Non-vegetated		
VIs	DVI	89.18±2.26	89.28±2.93	93.03±2.32	0.8567±0.03	90.44±2.08
	EVI	87.75±2.80	88.76±1.95	94.70±1.11	0.8568±0.02	90.52±1.39
	NDVI	91.13±2.93	87.44±3.50	95.14±2.68	0.8667±0.03	91.11±1.72
WIs	gNDVI	87.81±2.48	90.14±3.37	94.94±1.36	0.8629±0.03	90.86±1.66
	EWI	86.62±3.64	90.49±2.39	90.48±1.54	0.8346±0.02	88.97±1.11
	LSWI	95.07±1.67	83.71±3.86	88.43±2.80	0.8346±0.03	88.97±1.78
	NDWI	87.61±1.99	89.78±2.42	91.95±2.43	0.8454±0.02	89.69±1.28
MIs	RNDWI	88.69±1.55	90.35±2.01	89.91±3.18	0.8433±0.02	89.56±1.19
	CMRI	90.12±2.76	89.20±3.10	93.69±3.03	0.8693±0.03	91.31±1.70
	MVI	95.38±2.06	85.50±1.91	90.15±2.92	0.8538±0.02	90.25±1.50
	IMFI	88.82±3.12	93.38±2.28	90.70±2.65	0.8621±0.03	90.80±1.84
	NIMI	88.64±2.73	88.73±3.64	94.88±2.86	0.8596±0.03	90.64±2.09
GCMI (Ours)	GCMI (Ours)	96.12±1.14	89.78±1.94	89.95±4.06	0.8758±0.03	91.72±1.67

The results with bold typeface indicate the highest accuracies.

In each study area, one hundred training data for each mangrove, vegetation, and nonvegetated classes were independently selected to determine GCMI, which can avoid losing information of samples and increase the generalization performance of GCMI. The ST distances between the time series of different land covers were calculated according to (6), and the results are given in Table V. For WIs, the ST distances of LSWI and RNDWI are larger than the other two indices. As for VIs, the ST distances of EVI and gNDVI are larger than the other two indices. Therefore, the above four indices were selected to construct GCMI as

$$GCMI = \frac{A \times EVI + B \times gNDVI}{C \times LSWI + D \times RNDWI}. \quad (8)$$

2) Optimization of Undetermined Weights: Since the weights of the selected indices are unknown, we used PRGA to optimize weights, whose parameters were used in the algorithm given in Table VI. The optimal weights were obtained by PRGA, A = 3.4, B = 2.9, C = 4.3, and D = 1.1 (Table VII). Finally, GCMI was determined as

$$GCMI = \frac{3.4 \times EVI + 2.9 \times gNDVI}{4.3 \times LSWI + 1.1 \times RNDWI}. \quad (9)$$

We show the time series of GCMI in Fig. 8, where GCMI increases the separability between mangroves and other land covers significantly compared to that illustrated in Fig. 7. Besides, the trends of different land covers are quite different, which is quite useful for accurate classification.

C. Effectiveness of PRGA

In order to verify the effectiveness of PRGA, we compared the results with classical GA. Since GA is a heuristic algorithm, the result just running once is randomness. Therefore, the results

of classical GA and PRGA after running ten times respectively are listed in Table VII. According to the table, PRGA reaches the optimal result nine times out of ten runs, whereas classical GA only reaches the optimal result three times. Moreover, PRGA can get the optimal result in average around the 34th iteration. Therefore, PRGA can avoid trapping in local optimum and get the global optimal to some extent. However, the running time of PRGA increased by about 10% due to population reconstruction.

D. Effectiveness of ST Distance

To prove the effectiveness of ST distance, we compared Euclidean distance, Cosine distance, Pearson correlation coefficient, and DTW. The results of using different fitness functions in PRGA are reported in the Table VIII. In order to further verify the effectiveness of ST distance, the results of using the suboptimal parameters were also compared (Table IX). According to the results, ST distance yields the highest Kappa and OA. The OA is higher than Euclidean distance, Cosine distance, Pearson correlation coefficient, and DTW with 1%, 1.61%, 0.5% and 1% improvements, respectively. Comparing with the other suboptimal results, Kappa and OA are improved by about 0.014 and 1%, respectively, which clearly demonstrates the effectiveness of ST distance. Since GCMI does not consider the difference between vegetation and nonvegetated, the CA of vegetation and nonvegetated do not yield the highest, whereas the CA of mangrove is the highest. To sum up, regarding ST distance as fitness function can get the optimal result. Compared with Euclidean distance, Cosine distance, Pearson correlation coefficient, and DTW, ST distance can better measure the difference between time series.

E. Effectiveness of GCMI

To verify the effectiveness of GCMI, we compare the classification accuracies with the existing VIs, WIs, and MIs. The accuracies using time series of different indices are listed in the Table X. It is obvious that GCMI has the highest Kappa, OA, and the CA of mangrove, which demonstrated the effectiveness of GCMI. In VIs, NDVI obtained the highest Kappa and OA, which are around 0.0091 and 0.61% lower than GCMI, respectively. Besides, the CA of mangrove improved about 7.15% compared with that of VIs. In WIs, NDWI yielded the highest Kappa and OA, which are around 0.0304 and 2.03% lower than GCMI, respectively. Moreover, the CA of mangrove improved about 6.62% compared with WIs. As for MIs, the CA of mangrove improved 6, 0.74, 7.3 and 7.48%. Therefore, using the time series of GCMI to map mangroves could get the best classification result.

TABLE XI
ST DISTANCE OF DIFFERENT INDICES IN DONGZhai PORT AND QUANZHOU BAY

Dongzai Port				Quanzhou Bay			
Index	Mangrove vs. Vegetable	Index	Mangrove vs. Non-vegetated	Index	Mangrove vs. Vegetable	Index	Mangrove vs. Non-vegetated
EWI	0.209	DVI	1.094	EWI	2.879	DVI	8.943
LSWI	1.997	EVI	5.491	LSWI	2.720	EVI	7.966
NDWI	0.383	NDVI	1.219	NDWI	1.960	NDVI	11.535
RNDWI	0.213	gNDVI	2.727	RNDWI	3.635	gNDVI	13.180

The results with bold typeface indicate the highest accuracies.

TABLE XII
PARAMETERS OF PRGA IN DONGZhai PORT AND QUANZHOU BAY

Parameter	Site name	
	Dongzai Port	Quanzhou Bay
Maximum number of iteration	50	50
Population size	1000	1500
Maximum number of invalid iteration	3	3
Crossover rate	0.8	0.8
Mutation rate	0.03	0.03

TABLE XIII
GA OPTIMIZATION RESULTS IN DONGZhai PORT AND QUANZHOU BAY

Site	Method	Run	A	B	C	D	Fitness	Time (s)	#†
Dongzai Port	PRGA	1	0.7	4.7	2.8	2.7	14.317	952.76	43
		2	0.7	4.6	2.8	2.7	14.317	940.21	/
		3	0.7	4.7	2.8	2.7	14.317	957.84	14
		4	0.7	4.7	2.8	2.7	14.317	959.95	21
		5	0.7	4.7	2.8	2.7	14.317	948.65	21
		6	0.3	2	2.8	2.7	14.317	957.42	/
		7	0.7	4.7	2.8	2.7	14.317	972.35	17
		8	0.7	4.7	2.8	2.7	14.317	948.12	9
		9	0.7	4.7	2.8	2.7	14.317	942.43	23
		10	0.7	4.7	2.8	2.7	14.317	940.57	5
	GA	1	4.7	0.9	2.8	2.7	13.998	852.34	-
		2	5	1.6	2.8	2.7	13.997	871.39	-
		3	0.7	4.7	2.8	2.7	14.317	849.33	-
		4	3	0.3	2.8	2.7	13.998	827.46	-
		5	2.6	0.8	2.8	2.7	13.997	849.52	-
		6	5	0.8	2.9	2.8	13.343	855.56	-
		7	0.7	4.7	2.8	2.7	14.317	886.38	-
		8	1.7	0.3	2.8	2.7	13.998	825.54	-
		9	1.7	0.2	2.8	2.7	13.998	887.19	-
		10	5	1	2.8	2.8	13.998	864.42	-
Quanzhou Bay	PRGA	1	4.3	4.7	5	1.6	11.305	309.58	17
		2	2.1	2.3	5	1.6	11.305	306.96	/
		3	3.2	3.5	5	1.6	11.305	307.39	/
		4	4.3	4.7	5	1.6	11.305	306.49	32
		5	4.3	4.7	5	1.6	11.305	303.04	8
		6	2	2.2	5	1.6	11.305	304.92	/
		7	4.3	4.7	5	1.6	11.305	303.28	23
		8	4.3	4.7	5	1.6	11.305	301.78	29
		9	3.2	3.5	5	1.6	11.305	309	/
		10	4.3	4.7	5	1.6	11.305	298.21	18
	GA	1	3.2	1.9	4.8	1.4	11.291	274.67	-
		2	2.6	2.9	5	1.6	11.304	279.17	-
		3	2	1.2	4.8	1.4	11.291	280.51	-
		4	4.2	4.7	5	1.6	11.304	277.6	-
		5	3.1	3.5	5	1.6	11.304	274.28	-
		6	2.9	3.2	5	1.6	11.305	274.29	-
		7	2	1.2	4.8	1.5	11.291	279.54	-
		8	3.2	1.9	4.8	1.4	11.291	276.58	-
		9	4.3	4.7	5	1.6	11.305	277.21	-
		10	3.2	1.9	4.8	1.4	11.291	272.06	-

† The iteration reaching to the optimal result.

The results with bold typeface indicate the highest accuracies.

The classification results of different indices are shown in Fig. 9. It is obvious that GCMI can make full use of vegetation information and tidal inundation information of mangroves to get a better classification result. On the whole, for VIs and CMRI, we can see that nonmangrove vegetation is misclassified as mangroves in certain areas. For WIs, IMFI, and NIMI, we can see that nonvegetated is easily misclassified as mangroves in some regions. As for MVI, the mangroves adjoining to sea are easily misclassified.

For a clearer comparison, we chose two sites (A and B in Fig. 10) in Maowei Sea to show the clearer classification results

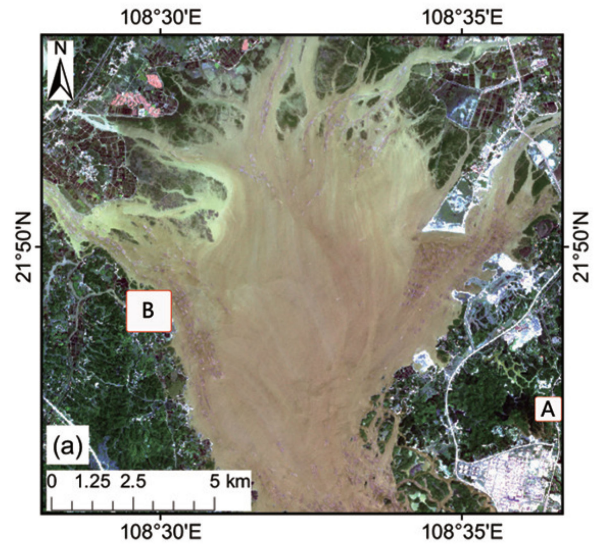


Fig. 10. Two local sites for comparison in Maowei Sea. Site A: Nonmangrove area. Site B: Mangrove area.

of mangrove. Fig. 11 shows the local area (A) where there is no mangrove distribution. It is obvious that excepting for GCMI and MVI, the other existing indices cannot distinguish vegetation and mangroves satisfactorily. Fig. 12 shows the mangrove classification result in local area (B) where there is mangrove distribution. By contrast, we can see VIs and MVI have omission errors in the boundary between sea and mangroves, which is due to the fact that mangroves are inundated by tidal periodically in this place where there have sparse vegetation information. What is more, since WIs, CMRI, IMFI, and NIMI did not consider the vegetation information, thus the water and some salt marsh plants are easily misclassified as mangroves.

V. DISSCUSSION

A. Advantages of the GCMI

This article presented a novel mangrove index GCMI based on VIs and WIs. Using the time series of GCMI to map mangroves, the obtained Kappa and OA can reach to 0.8758 and 91.72%, respectively. GCMI is the first mangrove index that considers both vegetation information and tidal inundation of mangroves based on time series. The advantages of GCMI are as follows:

- 1) Using phenology trajectory of mangrove. Mangrove is easily confused with terrestrial vegetation, but mangrove has phenological information of evergreen and tide

TABLE XIV
COMPARISON OF DIFFERENT FITNESS FUNCTIONS IN DONGZhai PORT AND QUANZHOU BAY

	Fitness function	(A, B, C, D)	CA/%			Kappa	OA/%
			Mangrove	Vegetation	Non-vegetated		
Dongzhai Port	Euclidean distance	(5.0, 5.0, 0.3, 0.2)	87.13±2.75	90.10±2.49	94.46±1.27	0.8627±0.02	90.96±1.04
	Cosine distance	(0.1, 5.0, 4.3, 4.5)	87.18±2.86	89.77±2.32	94.38±1.25	0.8593±0.02	90.73±1.38
	Pearson correlation	(0.3, 3.8, 3.4, 1.4)	86.78±2.92	87.08±1.74	93.63±1.84	0.8364±0.01	89.23±0.82
	Pearson correlation	(0.3, 3.8, 1.7, 0.7)	86.19±3.27	89.75±1.76	94.46±1.29	0.8540±0.01	90.38±0.64
	DTW distance	(5.0, 5.0, 0.3, 0.2)	86.41±1.85	85.53±1.94	93.51±1.80	0.8257±0.01	88.59±0.80
	ST distance	(0.7, 4.7, 2.7, 2.8)	87.68±1.67	92.09±2.68	94.67±2.55	0.8667±0.02	91.21±1.49
Quanzhou Bay	Euclidean distance	(5.0, 5.0, 4.3, 1.8)	93.42±3.41	86.05±3.15	89.39±3.54	0.8387±0.02	89.25±1.61
	Cosine distance	(0.1, 5.0, 3.8, 1.9)	88.96±3.74	91.20±3.92	84.13±4.29	0.8332±0.04	88.88±2.68
	Pearson correlation	(0.3, 3.8, 1.7, 0.7)	91.87±3.83	89.96±3.35	89.11±2.66	0.8519±0.03	90.08±2.14
	DTW distance	(5.0, 5.0, 4.3, 1.8)	93.42±3.41	86.05±3.15	89.39±3.54	0.8387±0.02	89.25±1.61
	ST distance	(4.3, 4.7, 5.0, 1.6)	95.43±1.53	89.32±2.94	90.43±2.57	0.8705±0.02	91.43±1.64

The results with bold typeface indicate the highest accuracies.

TABLE XV
COMPARISON OF DIFFERENT INDEX IN DONGZhai PORT AND QUANZHOU BAY

		Index	CA/%			Kappa	OA/%
			Mangrove	Vegetation	Non-vegetated		
Dongzhai Port	VIs	DVI	78.70±3.23	85.18±2.67	96.36±1.74	0.8090±0.03	87.42±1.79
		EVI	81.23±4.37	84.00±2.43	95.00±1.49	0.8062±0.02	87.25±1.45
		NDVI	80.77±3.15	86.86±2.57	94.41±2.03	0.8174±0.02	88.00±1.34
		gNDVI	80.50±2.95	85.43±3.54	95.00±4.80	0.8120±0.02	87.65±1.05
	WIs	EWI	82.80±2.64	87.53±2.16	94.77±1.54	0.8317±0.02	88.94±1.37
		LSWI	87.07±2.78	86.26±1.92	89.09±2.41	0.8258±0.02	88.54±1.51
		NDWI	82.41±2.66	86.83±2.82	96.29±0.69	0.8344±0.02	89.11±1.09
		RNDWI	84.78±3.35	90.49±2.51	94.48±0.65	0.8537±0.02	90.38±1.20
	MIs	CMRI	80.46±3.00	82.83±3.04	96.37±1.63	0.8091±0.02	87.44±1.01
		MVI	86.39±1.87	87.54±1.60	92.17±1.56	0.8307±0.01	88.86±0.98
		IMFI	82.64±2.67	85.48±1.99	95.2±3.67	0.8272±0.01	88.65±0.91
		NIMI	84.42±2.57	86.31±1.82	95.37±1.52	0.8349±0.02	89.15±1.32
	GCMI (Ours)		87.68±1.67	92.09±2.68	94.67±2.55	0.8667±0.02	91.21±1.49
Quanzhou Bay	VIs	DVI	86.02±5.03	82.08±3.11	98.37±1.40	0.8275±0.30	88.50±2.03
		EVI	85.77±4.42	81.63±3.62	96.13±2.78	0.8156±0.04	87.71±2.67
		NDVI	85.63±3.09	82.45±5.17	98.01±1.45	0.8269±0.04	88.46±2.54
		gNDVI	84.78±3.51	84.17±3.90	95.64±4.01	0.8219±0.03	88.12±2.16
	WIs	EWI	90.45±1.71	82.59±4.90	90.36±3.06	0.8116±0.03	87.38±2.11
		LSWI	93.94±2.53	80.41±3.72	91.38±2.80	0.8175±0.03	87.83±2.19
		NDWI	90.01±5.32	83.51±2.91	93.13±2.27	0.8306±0.03	88.71±2.03
		RNDWI	91.07±4.86	85.73±3.21	89.81±3.27	0.8450±0.03	89.67±2.19
	MIs	CMRI	86.25±4.90	82.75±3.26	97.93±1.78	0.8344±0.04	88.96±2.44
		MVI	93.32±1.84	83.41±4.43	94.75±3.03	0.8501±0.03	90.04±1.82
		IMFI	90.42±2.46	86.03±2.29	95.05±3.67	0.8528±0.03	90.70±1.71
		NIMI	88.47±2.86	86.25±2.18	97.51±1.96	0.8593±0.02	91.10±0.96
	GCMI (Ours)		95.43±1.53	89.32±2.94	90.43±2.57	0.8705±0.02	91.43±1.64

The results with bold typeface indicate the highest accuracies.

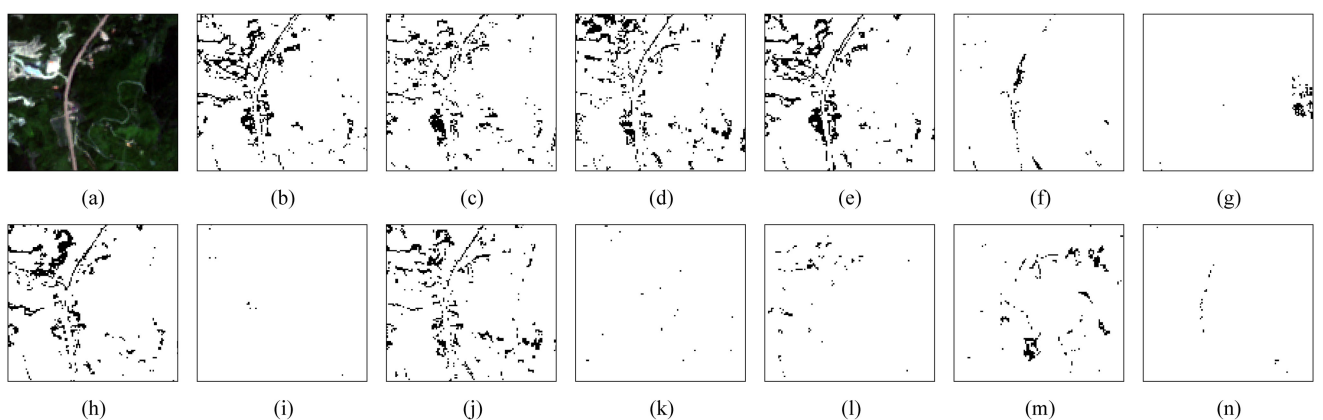


Fig. 11. Mangroves information of site A in Maowei Sea. (a) Site A; (b) DVI; (c) EVI; (d) NDVI; (e) gNDVI; (f) EWI; (g) LSWI; (h) NDWI; (i) RNDWI; (j) CMRI; (k) MVI; (l) IMFI; (m) NIMI; and (n) GCMI.

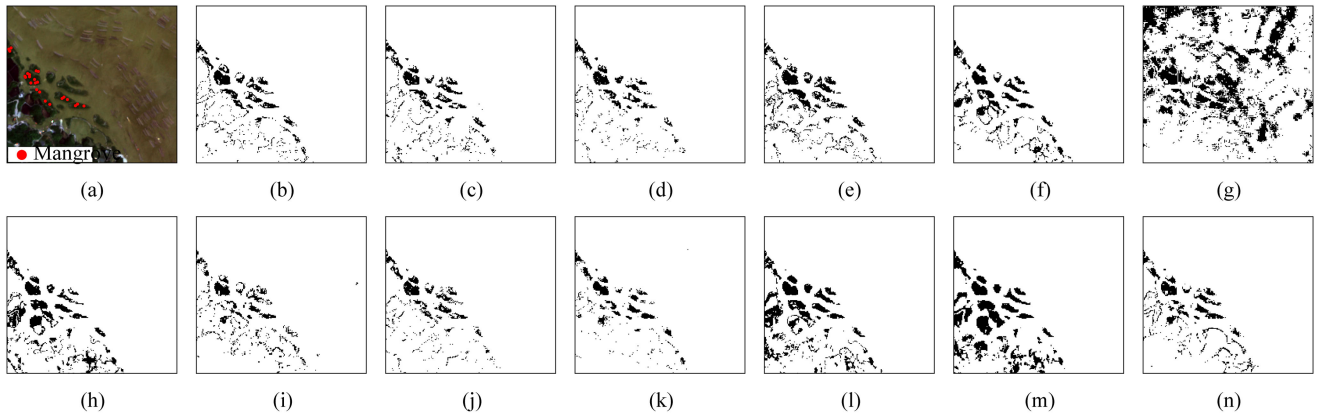


Fig. 12. Mangroves information of site B in Maowei Sea. (a) Site B. (b) DVI. (c) EVI. (d) NDVI. (e) gNDVI. (f) EWI. (g) LSWI. (h) NDWI. (i) RNDWI. (j) CMRI. (k) MVI. (l) IMFI. (m) NIMI. (n) GCMI.

inundation, which can be used to distinguish it from other land covers.

- 2) Regarding ST distance as the criterion to measure the separability of time series. ST distance refers to the multi-criteria judgment, which evaluates the similarity and trend of time series at the same time. In this article, ST distance helps to confirm the indices and weights in GCMI. The precision of using ST distance is the highest compared with Euclidean distance, Cosine distance, Pearson correlation coefficient, and DTW, which proves the reliability of ST distance.
- 3) Using PRGA to optimize weights involved in GCMI. Depending on the module of reconstructing population, the probability of getting the global optimum can be increased by about 55%. However, the running time of PRGA is about 10% higher than classical GA, because population would be reconstructed when reach the number of max invalid iteration.

Different from the existing normalized index, the weights of GCMI are more interpretable and can be more useful to distinguish mangroves from other land covers.

B. Application to Other Study Areas

GCMI was utilized to test the performance of mapping mangroves in other study areas, i.e., Dongzhai Port and Quanzhou Bay. Firstly, the indices with higher difference of time series were selected. Table XI reports ST distance between different indices, where LSWI, NDWI, EVI, and gNDVI were selected for Dongzhai Port, whereas EWI, RNDWI, NDVI, and gNDVI were selected for Quanzhou Bay. Secondly, PRGA was used to optimize the undetermined weights and the parameters used in PRGA are listed in Table XII. Similarly, we compared the optimization results of classical GA and PRGA (see Table XIII). From Table XIII, it can be seen that PRGA has a more robust ability to get the global optimal result. Finally, GCMI in Dongzhai Port and Quanzhou Bay were defined as (10) and (11), respectively

$$GCMI = \frac{0.7 \times EVI + 4.7 \times gNDVI}{2.8 \times LSWI + 2.7 \times NDWI} \quad (10)$$

$$GCMI = \frac{4.3 \times NDVI + 4.7 \times gNDVI}{5.0 \times EWI + 1.6 \times RNDWI}. \quad (11)$$

After constructing the index, accuracies are reported in Tables XIV and XV. From Table XIV, it can be seen that ST distance yields the highest Kappa, OA, and CA of mangrove. In DongZhai Port, the OA of ST distance is higher than that of Euclidean distance, Cosine distance, Pearson correlation coefficient, and DTW, with 0.25%, 0.48%, 1.41%, and 2.62% improvements, respectively. In QuanZhou Bay, the OA of ST distance is higher than that of Euclidean distance, Cosine distance, Pearson correlation coefficient, and DTW with 2.18%, 2.55%, 1.35%, and 2.8% improvements, respectively. According to Table XV, GCFI has the highest Kappa, OA and CA of mangrove, which demonstrated the effectiveness of GCFI. In DongZhai Port, the OA of GCFI improved 3.63%, 1.97%, and 2.69% comparing with VIs, WIs, and MIs, respectively. In QuanZhou Bay, the OA of GCFI improved 3.23%, 3.03%, and 1.23% comparing with VIs, WIs, and MIs, respectively. What's more, the classification results in DongZhai Port and QuanZhou Bay are shown in Fig. 13. Since spartina alterniflora was introduced in Quanzhou Bay in 1982, and it has had a great negative impact on the ecosystem, affecting the growth of mangroves seriously. Therefore, mangrove in Quanzhou Bay is sparsely distributed, as shown in Fig. 13(b). The results in DongZhai Port and QuanZhou Bay demonstrate the effectiveness of ST distance, validity of PRGA, and universality of GCFI.

C. Prospects

In this article, we demonstrate that GCFI time series can be efficiently used for mangrove mapping in South China coastal region. GCFI enhances the separability between mangrove and other land covers by taking full advantage of its vegetation information and tide inundation information. However, GCFI still requires further study and improvement in the future work. Currently, the phenological information contained in time series has not been fully explored since they are directly used as features for classification. Therefore, mining the phenological information from time series may achieve better classification results.

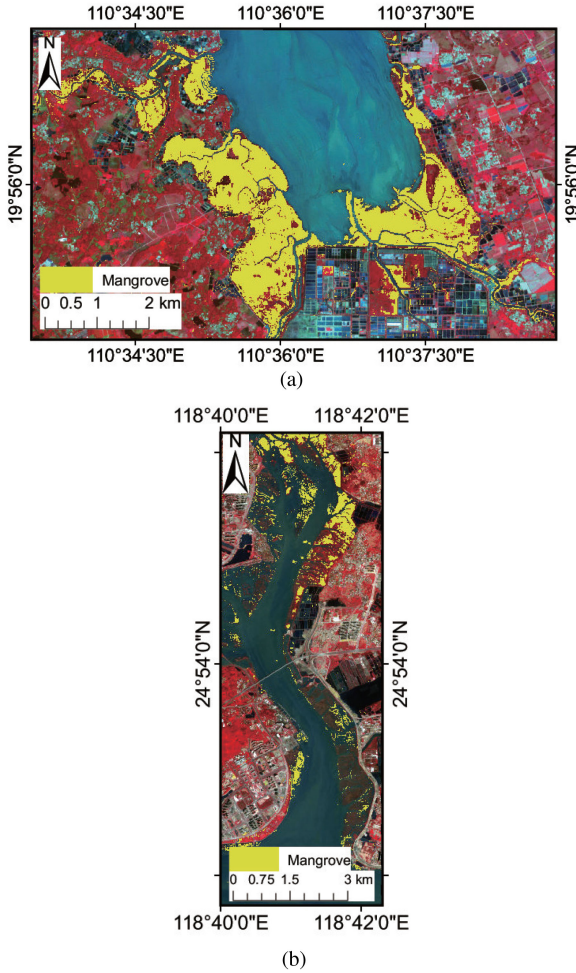


Fig. 13. Mangrove mapping in (a) Dongzhai Port and (b) Quanzhou Bay.

VI. CONCLUSION

In this article, we proposed a new mangrove index, namely GCMI based on Sentinel-2 data. Firstly, GCMI was built by compositing indices selected by using ST distance. Then, the weights of GCMI were optimized by PRGA. Finally, the time series of GCMI were regarded as features to map mangroves by using RF. Taking south China coastal regions as study areas, the mainly results are given as follows:

- 1) The classification results show that GCMI enhances the separability between mangroves and other land covers compared to existing VIs, WIs, and MIs. Using the GCMI time series to map mangrove in Maowei Sea, the kappa and OA are 0.8758 and 91.72%, respectively.
- 2) ST distance jointly evaluates the similarity and trend of time series, which is more suitable for measuring the differences between time series. ST distance produces about 1, 1.61, 0.5, and 1% improvements in terms of OA compared to Euclidean distance, Cosine distance, Pearson correlation coefficient, and DTW, respectively.
- 3) PRGA has greater capability to obtain the optimal result since it can maintain the diversity in population. The average probability of getting the global optimum within

ten times is 70%, whereas the average probability is only 16% when using classical GA.

This article develops GCMI based on existing indices, and GCMI time series show superior performance in mapping mangroves. The method is novel and propagable, which can be used for mangroves mapping in other sites. What is more, the 10-m mangrove map can provide support for coastal management and decision basis to protect mangrove.

The innovative contributions of this study are as follows.

- 1) We proposed GCMI by compositing existing VIs and WIs based on time series. Compared with other MIs, GCMI cannot only fully make use of the information from phenological trajectories, but also distinguish mangroves from other vegetation and nonvegetated simultaneously.
- 2) We designed ST distance to measure the time series differences. Different from the other distance measures, ST distance can consider both similarity and trend of time series.
- 3) We improved the classical GA by reconstructing population to optimize the parameters in GCMI. PRGA has more robust ability to get the optimal result in contrast to the classical method.

Currently, the phenological information contained in time series has not been fully explored since they are directly used as features for classification. Therefore, in our future work, we will exploit the phenological information from time series, which may achieve better classification results.

ACKNOWLEDGMENT

The authors would like to thank X. Han *et al.* for making the 10-m Global Mangrove Classification products during 2018–2020 available in this research field, and also thank C. Zhao and C. Qin for sharing their sample datasets.

REFERENCES

- [1] N. J. Murray *et al.*, “The global distribution and trajectory of tidal flats,” *Nature*, vol. 565, no. 7738, pp. 222–225, 2019.
- [2] M. Schuerch *et al.*, “Future response of global coastal wetlands to sea-level rise,” *Nature*, vol. 561, no. 7722, pp. 231–234, 2018.
- [3] P. I. Macreadie *et al.*, “The future of Blue Carbon science,” *Nature Commun.*, vol. 10, no. 1, pp. 1–13, 2019.
- [4] L. Goldberg, D. Lagomasino, N. Thomas, and T. Fatoyinbo, “Global declines in human-driven mangrove loss,” *Glob. Change Biol.*, vol. 26, no. 10, pp. 5844–5855, 2020.
- [5] H. Lin and H. Zhang, “Tropical and subtropical remote sensing: Needs, challenges, and opportunities,” *Nat. Remote Sens. Bull.*, vol. 25, no. 01, pp. 276–291, 2021.
- [6] L. Wang, M. Jia, D. Yin, and J. Tian, “A review of remote sensing for mangrove forests: 1956–2018,” *Remote Sens. Environ.*, vol. 231, 2019, Art. no. 11223.
- [7] T. D. Pham, N. Yokoya, D. T. Bui, K. Yoshino, and D. A. Friess, “Remote sensing approaches for monitoring mangrove species, structure, and biomass: Opportunities and challenges,” *Remote Sens.*, vol. 11, no. 3, 2019, Art. no. 230.
- [8] Z. Zhou *et al.*, “Review on dynamic monitoring of mangrove forestry using remote sensing,” *J. Geo-Inf. Sci.*, vol. 20, no. 11, pp. 1631–1643, 2018.
- [9] W. Hu *et al.*, “Mapping the potential of mangrove forest restoration based on species distribution models: A case study in China,” *Sci. Total Environ.*, vol. 748, 2020, Art. no. 142321.
- [10] H. Li, M. Jia, R. Zhang, Y. Ren, and X. Wen, “Incorporating the plant phenological trajectory into mangrove species mapping with dense time series Sentinel-2 imagery and the Google Earth Engine platform,” *Remote Sens.*, vol. 11, no. 21, 2019, Art. no. 2479.

- [11] T. D. Pham *et al.*, "Estimating mangrove above-ground biomass using extreme gradient boosting decision trees algorithm with fused Sentinel-2 and ALOS-2 PALSAR-2 data in can Gio biosphere reserve, Vietnam," *Remote Sens.*, vol. 12, no. 5, 2020, Art. no. 777.
- [12] J. A. A. Castillo, A. A. Apan, T. N. Maraseni, and S. G. Salmo III, "Estimation and mapping of above-ground biomass of mangrove forests and their replacement land uses in the Philippines using Sentinel imagery," *ISPRS J. Photogrammetry Remote Sens.*, vol. 134, pp. 70–85, 2017.
- [13] P. Mondal, X. Liu, T. E. Fatoyinbo, and D. Lagomasino, "Evaluating combinations of Sentinel-2 data and machine-learning algorithms for mangrove mapping in West Africa," *Remote Sens.*, vol. 11, no. 24, 2019, Art. no. 2928.
- [14] W. Li and M. Hughes, "Coastal wetland mapping using ensemble learning algorithms: A comparative study of bagging, boosting and stacking techniques," *Remote Sens.*, vol. 12, no. 10, May 2020, Art. no. 1683.
- [15] A. Navarro, M. Young, P. I. Macreadie, E. Nicholson, and D. Ierodiaconou, "Mangrove and saltmarsh distribution mapping and land cover change assessment for South-eastern Australia from 1991 to 2015," *Remote Sens.*, vol. 13, no. 8, 2021, Art. no. 1450.
- [16] X. Liu *et al.*, "Large-scale high-resolution coastal mangrove forests mapping across West Africa with machine learning ensemble and satellite Big Data," *Front. Earth Sci.*, vol. 8, 2021, Art. no. 677.
- [17] C. Nwobi, M. Williams, and E. T. Mitchard, "Rapid mangrove forest loss and nipa palm (nypa fruticans) expansion in the Niger Delta, 2007–2017," *Remote Sens.*, vol. 12, no. 14, 2020, Art. no. 2344.
- [18] N. H. Quang *et al.*, "Multi-decadal changes in mangrove extent, age and species in the red river estuaries of Viet Nam," *Remote Sens.*, vol. 12, no. 14, 2020, Art. no. 2289.
- [19] L. Duarte, P. Silva, and A. C. Teodoro, "Development of a QGIS plugin to obtain parameters and elements of plantation trees and vineyards with aerial photographs," *ISPRS Int. J. Geo-Inf.*, vol. 7, no. 3, 2018, Art. no. 109.
- [20] X. Zhang, P. M. Treitz, D. Chen, C. Quan, L. Shi, and X. Li, "Mapping mangrove forests using multi-tidal remotely-sensed data and a decision-tree-based procedure," *Int. J. Appl. Earth Observation Geoinformation*, vol. 62, pp. 201–214, 2017.
- [21] M. J. McCarthy *et al.*, "Automated high-resolution time series mapping of mangrove forests damaged by hurricane Irma in Southwest Florida," *Remote Sens.*, vol. 12, no. 11, 2020, Art. no. 1740.
- [22] C. Iovan, M. Kulwicki, and E. Mermet, "Deep convolutional neural network for mangrove mapping," in *Proc. IEEE Int. Geosci. Remote Sens. Symp.*, 2020, pp. 1969–1972.
- [23] M. Guo, Z. Yu, Y. Xu, Y. Huang, and C. Li, "Me-Net: A deep convolutional neural network for extracting mangrove using Sentinel-2 A data," *Remote Sens.*, vol. 13, no. 7, 2021, Art. no. 1292.
- [24] Y. Yuan, L. Lin, Q. Liu, R. Hang, and Z.-G. Zhou, "Sits-former: A pre-trained spatio-spectral-temporal representation model for sentinel-2 time series classification," *Int. J. Appl. Earth Observation Geoinformation*, vol. 106, 2022, Art. no. 102651.
- [25] L. Lymburner *et al.*, "Mapping the multi-decadal mangrove dynamics of the Australian coastline," *Remote Sens. Environ.*, vol. 238, 2020, Art. no. 111185.
- [26] D. Wang *et al.*, "Evaluating the performance of Sentinel-2, Landsat 8 and Pléiades-1 in mapping mangrove extent and species," *Remote Sens.*, vol. 10, no. 9, 2018, Art. no. 1468.
- [27] Q. Li, F. K. K. Wong, and T. Fung, "Mapping multi-layered mangroves from multispectral, hyperspectral, and LiDAR data," *Remote Sens. Environ.*, vol. 258, 2021, Art. no. 112403.
- [28] P. Bunting *et al.*, "The global mangrove watch-A new 2010 global baseline of mangrove extent," *Remote Sens.*, vol. 10, no. 10, 2018, Art. no. 1669.
- [29] J. Pastor-Guzman, J. Dash, and P. M. Atkinson, "Remote sensing of mangrove forest phenology and its environmental drivers," *Remote Sens. Environ.*, vol. 205, pp. 71–84, 2018.
- [30] L. Hu, N. Xu, J. Liang, Z. Li, L. Chen, and F. Zhao, "Advancing the mapping of mangrove forests at national-scale using Sentinel-1 and Sentinel-2 time-series data with Google Earth Engine: A case study in China," *Remote Sens.*, vol. 12, no. 19, 2020, Art. no. 3120.
- [31] B. Chen *et al.*, "A mangrove forest map of China in 2015: Analysis of time series Landsat 7/8 and Sentinel-1 A imagery in Google Earth Engine cloud computing platform," *ISPRS J. Photogrammetry Remote Sens.*, vol. 131, pp. 104–120, 2017.
- [32] C. Zhao and C.-Z. Qin, "10-m-resolution mangrove maps of China derived from multi-source and multi-temporal satellite observations," *ISPRS J. Photogrammetry Remote Sens.*, vol. 169, pp. 389–405, 2020.
- [33] A. Ghorbanian, S. Zaghan, R. M. Asiyabi, M. Amani, A. Mohammadzadeh, and S. Jamali, "Mangrove ecosystem mapping using Sentinel-1 and Sentinel-2 satellite images and random forest algorithm in Google Earth Engine," *Remote Sens.*, vol. 13, no. 13, 2021, Art. no. 2565.
- [34] C. J. Tucker, "Red and photographic infrared linear combinations for monitoring vegetation," *Remote Sens. Environ.*, vol. 8, no. 2, pp. 127–150, 1979.
- [35] J. M. Chen and T. Black, "Defining leaf area index for non-flat leaves," *Plant, Cell Environ.*, vol. 15, no. 4, pp. 421–429, 1992.
- [36] K. Gupta *et al.*, "An index for discrimination of mangroves from non-mangroves using LANDSAT 8 OLI imagery," *MethodsX*, vol. 5, pp. 1129–1139, 2018.
- [37] A. B. Baloloy, A. C. Blanco, R. R. C. S. Ana, and K. Nadaoka, "Development and application of a new mangrove vegetation index (MVI) for rapid and accurate mangrove mapping," *ISPRS J. Photogrammetry Remote Sens.*, vol. 166, pp. 95–117, 2020.
- [38] M. Jia, Z. Wang, Y. Zhang, D. Mao, and C. Wang, "Monitoring loss and recovery of mangrove forests during 42 years: The achievements of mangrove conservation in China," *Int. J. Appl. Earth Observation Geoinformation*, vol. 73, pp. 535–545, 2018.
- [39] Q. Xia, C.-Z. Qin, H. Li, C. Huang, and F.-Z. Su, "Mapping mangrove forests based on multi-tidal high-resolution satellite imagery," *Remote Sens.*, vol. 10, no. 9, 2018, Art. no. 1343.
- [40] W. Li, H. El-Askary, M. A. Qurban, J. Li, K. ManiKandan, and T. Piechota, "Using multi-indices approach to quantify mangrove changes over the Western Arabian Gulf along Saudi Arabia coast," *Ecological Indicators*, vol. 102, pp. 734–745, 2019.
- [41] F. Xu, Y. Zhang, L. Zhai, J. Liu, and X. Gu, "Extraction method of intertidal mangrove by using Sentinel-2 images," *Bull. Surveying Mapping*, no. 2, pp. 49–54, 2020.
- [42] T. Kumar, A. Mandal, D. Dutta, R. Nagaraja, and V. K. Dadhwal, "Discrimination and classification of mangrove forests using EO-1 hyperion data: A case study of Indian Sundarbans," *Geocarto Int.*, vol. 34, no. 4, pp. 415–442, 2019.
- [43] R. Xu, S. Zhao, and Y. Ke, "A simple phenology-based vegetation index for mapping invasive spartina alterniflora using Google Earth Engine," *IEEE J. Sel. Topics Appl. Earth Observ. Remote Sens.*, vol. 14, pp. 190–201, 2021.
- [44] W. Wang, H. Fu, S. Y. Lee, H. Fan, and M. Wang, "Can strict protection stop the decline of mangrove ecosystems in China? From rapid destruction to rampant degradation," *Forests*, vol. 11, no. 1, p. 55, 2020.
- [45] H. Xiao *et al.*, "10-m global mangrove classification products of 2018–2020 based on big data," *Science Data Bank*, Aug. 12, 2021, Accessed: Jun. 27, 2022. [Online]. Available: <http://doi.org/10.11922/sciencedb.01019>
- [46] Z. Chuanpeng and Q. Chengzhi, "A sample dataset of coastal land cover including mangroves in southern China," *Science Data Bank*, Jun. 15, 2022, Accessed: Jun. 27, 2022. [Online]. Available: <http://doi.org/10.11922/sciencedb.00279>
- [47] A. Huete, K. Didan, T. Miura, E. P. Rodriguez, X. Gao, and L. G. Ferreira, "Overview of the radiometric and biophysical performance of the MODIS vegetation indices," *Remote Sens. Environ.*, vol. 83, no. 1/2, pp. 195–213, 2002.
- [48] C. F. Jordan, "Derivation of leaf-area index from quality of light on the forest floor," *Ecology*, vol. 50, no. 4, pp. 663–666, 1969.
- [49] A. A. Gitelson and M. N. Merzlyak, "Remote sensing of Chlorophyll concentration in higher plant leaves," *Adv. Space Res.*, vol. 22, no. 5, pp. 689–692, 1998.
- [50] X. Xiao *et al.*, "Satellite-based modeling of gross primary production in an evergreen needleleaf forest," *Remote Sens. Environ.*, vol. 89, no. 4, pp. 519–534, 2004.
- [51] S. K. McFeeters, "The use of the normalized difference water index (NDWI) in the delineation of open water features," *Int. J. Remote Sens.*, vol. 17, no. 7, pp. 1425–1432, 1996.
- [52] Y. Pei, Y.-j. ZHANG, and Z. Yuan, "A study on information extraction of water system in semi-arid regions with the enhanced water index (EWI) and GIS based noise remove techniques," *Remote Sens. Inf.*, vol. 6, pp. 62–67, 2007.
- [53] C. Rong-long, L. Cun-jun, L. Liang-yun, W. Ji-hua, and Y. Guang-jian, "Extracting Miyun reservoir's water area and monitoring its change based on a revised normalized different water index," *Sci. Surveying Mapping*, vol. 33, pp. 158–160, 2008.
- [54] P. Senin, "Dynamic time warping algorithm review," *Information and Computer Science Department University of Hawaii at Manoa Honolulu, USA*, vol. 855, no. 1–23, p. 40, 2008.

- [55] D. Whitley, "A genetic algorithm tutorial," *Statist. Comput.*, vol. 4, no. 2, pp. 65–85, 1994.
- [56] M. Kaya, "The effects of a new selection operator on the performance of a genetic algorithm," *Appl. Math. Computation*, vol. 217, no. 19, pp. 7669–7678, 2011.
- [57] S. Katoch, S. S. Chauhan, and V. Kumar, "A review on genetic algorithm: Past, present, and future," *Multimedia Tools Appl.*, vol. 80, pp. 1–36, 2020.
- [58] S. Manikandan, K. Ramar, M. W. Iruthayaraajan, and K. Srinivasagan, "Multilevel thresholding for segmentation of medical brain images using real coded genetic algorithm," *Measurement*, vol. 47, pp. 558–568, 2014.
- [59] S. Talukdar *et al.*, "Land-use land-cover classification by machine learning classifiers for satellite observations—A review," *Remote Sens.*, vol. 12, no. 7, 2020, Art. no. 1135.



Zhaohui Xue (Member, IEEE) received the B.S. degree in geomatics engineering from Shandong Agricultural University, Tai'an, China, the M.E. degree in remote sensing from the China University of Mining and Technology, Beijing, China, and the Ph.D. degree in cartography and geographic information system from Nanjing University, Nanjing, China, in 2009, 2012, and 2015, respectively.

He is currently a Youth Professor (Ph.D. supervisor) with the School of Earth Sciences and Engineering, Hohai University, Nanjing, China. He has authored nearly 50 scientific papers, including 26 SCI papers with JCR Q1 and Q2. His research interests include hyperspectral image classification, time-series image analysis, pattern recognition, and machine learning.

Dr. Xue was a recipient of the National Scholarship for Doctoral Graduate Students granted by the Ministry of Education of the People's Republic of China in 2014. He was awarded the Best Reviewer for the *IEEE Geoscience and Remote Sensing Society*. He is an editorial board member in *National Remote Sensing Bulletin* (2020–2024). He has been a reviewer for more than ten famous remote sensing journals including *IEEE TRANSACTIONS ON GEOSCIENCE AND REMOTE SENSING* and *ISPRS Journal of Photogrammetry and Remote Sensing*.



Siyu Qian received the B.S. degree in geomatics engineering from the Zhejiang University of Water Resources and Electric Power, Hangzhou, China, in 2020. She is currently working toward the M.E. degree in surveying and mapping engineering with Hohai University, Nanjing, China.

Her research interests include time-series image analysis and wetland classification using remote sensing.